BAlGaN-based Vertical Cavity Surface Emitting Laser Operating in Deep UV Region

X. Li[1,2], S. Sundaram[2], P. Disseix[3], S. Bouchoule[4], G. Le Gac[3], G. Patriarche[4], F. Réveret[3], J. Leymarie[3], Y. El Gmili[2], J. Streque[2], F. Genty[5], J-P. Salvestrini[2,6], P. L. Voss[1,2], R. D. Dupuis[7] and A. Ougazzaden[1,2]

[1]*School of Electrical and Computer Engineering, Georgia Institute of Technology, GT-Lorraine, 57070 Metz, France*
[2]*UMI 2958, Georgia Tech - CNRS, 57070 Metz, France*
[3]*Institut Pascal UMR 6602 CNRS, Université Blaise Pascal, 63171 Aubière, France*
[4]*LPN CNRS, UPR20, 91460 Marcoussis, France*
[5]*Supelec, LMOPS, EA4423, 57070 Metz, France*
[6]*Université de Lorraine, LMOPS, EA 4423, 57070 Metz, France*
[7]*Center for Compound Semiconductors and School of Electrical and Computer Engineering, Georgia Institute of Technology, Atlanta, Georgia 30332, U.S.A.*

1 RESEARCH PROBLEM

There is a strong demand for semiconductor light sources emitting in the DUV region for a wide variety of potential applications such as sterilization, water/air purification, optical imaging systems, spectroscopy, or high density storage systems. However, the primary limitation of current applications is the existing UV sources. The conventional UV light sources are excimer lasers, mercury lamps or Nd: YAG lasers. These sources suffer from low level of performance, low reliability, significant size, and the toxic substances. Compared with conventional lasers, the semiconductor light-emitting devices are an ideal choice due to their reliability, compactness and high efficiency. Besides, the wavelength could be tuned by changing the compositions of the active region. UV semiconductor light sources are of great technological interest in our daily lives.

Among semiconductor laser devices, VCSEL is one of the most attractive configurations: The emission light from VCSEL is perpendicular to the surface, so it could be integrated into two dimensional arrays. 10000 devices could be integrated on one wafer to give high output. Circular beam makes it easy for coupling into the fiber. It consists of high reflectivity distributed Bragg reflector (DBR) mirrors, which enables low threshold and high output. Besides, it could be tested during processing which decreases the manufacturing cost. Compared with EELs, it has low temperature sensitivity due to its single longitudinal cavity.

AlGaInN-based wide bandgap semiconductor material systems have brought innovative changes in photonic devices, which allow the operating wavelengths of LEDs and lasers to reach a spectral range spanning from blue to DUV. However, the III-nitride VCSELs demonstrated so far operate in the wavelengths of visible violet and blue spectral range, while no efficient VCSELs emitting below 300 nm were reported. To extend the VCSEL emission to the ultraviolet region, the challenges lie in many aspects. Firstly, there is a degradation of the structural quality of heteroepitaxial AlGaN materials with increasing Al molar ratio and lack of high quality AlN substrates. High dislocation density for the structure grown on foreign substrates would lead to low internal quantum efficiency (IQE). Secondly, AlGaN MQWs suffer from the strong quantum-confined Stark effect (QCSE) induced by piezoelectric and spontaneous polarization, which leads to the separation of electrons and holes and reduces significantly the emission efficiency. C-plane AlGaN alloys also exhibit anisotropic optical polarization properties: E-field $\perp$ c polarized emission (which will be referred to as TE polarization) decreases when compared to the emission polarized along the c axis (E-field // c) as the Al composition increases for the deep UV wavelengths, which is harmful to surface-emission. Thirdly, high-reflectivity distributive Bragg reflector

LI X., Sundaram S., Disseix P., Bouchoule S., Le Gac G., Patriarche G., Réveret F., Leymarie J., Gmili Y., Streque J., Genty F., Salvestrini J., Voss P., Dupuis R. and Ougazzaden A..
BAlGaN-based Vertical Cavity Surface Emitting Laser Operating in Deep UV Region.

(DBR) with large bandwidth for the DUV VCSELs is a big challenge, considering the limited refractive index contrast and large lattice mismatch for conventionally used AlGaN/Al(Ga)N structures.

Based on the challenges mentioned above, in the framework of developing DUV VCSELs for this work, TE-emission enhanced AlGaN MQWs emitting at 280 nm grown on relaxed AlGaN buffer, new BAlN material system which can have big refractive index contrast with Al(Ga)N and its applications to DBRs would be studied and explored.

2 OUTLINE OF OBJECTIVES

The objective of this thesis is to develop efficient vertical cavity surface-emitting lasers operating below 300 nm. The final structure consists of dielectric top mirror, AlGaN active region and bottom DBR based on BAlGaN material system.

The first part of the work is addressed to the AlGaN active region, including the study of AlGaN epitaxial growth for the control of composition and strain relaxation, the realization of TE-enhanced MQWs design and the related characterizations. The purpose is to develop efficient DUV MQWs with improved TE emission.

The second part focuses on the growth of novel BAlN material, in order to study the influence of growth conditions and characteristics of the material.

The third part would be the design and realization of DBRs, including both BAlGaN DBRs and conventional AlGaN DBRs as reference.

The final goal is to realize DUV devices: laser diodes, RC-LEDs and ultimate VCSELs.

3 STATE OF THE ART

Visible and UV-VCSELs and edge-emitting lasers (EELs) based upon the wide bandgap semiconductors including ZnSe- and GaN-based material systems have been extensively explored for the potential applications of high density optical storage system, laser printer engines, full color display systems, and large-area projector systems. The ZnSe-based materials were the first material system to provide continuous wave operation of blue-green EELs (Ding et al. 1990). However, serious reliability problems possibly arising from its chemically and structurally unstable material system, have hindered the application of ZnSe lasers in the real-world systems. Later, AlGaInN-based wide bandgap semiconductor material systems (Gil 1998; McIntosh et al. 1996) have brought innovative changes in photonic devices, which enable the operating wavelengths of LEDs and lasers to reach a spectral range from blue to UV (Shatalov et al. 2002). The first nitride-based injection laser centered at around 390 nm was demonstrated in 1995 (Akasaki et al. 1995). AlGaN-based UV LEDs for wavelength shorter than 360 nm was initiated in 1998 (Han et al. 1998). Then UV and DUV light devices have undergo tremendous evolution through rapid progress in material growth, device fabrication and packaging. In the DUV range, the LEDs and EELs have progressed a lot. The group of Sensor Electric Technology has reported high external quantum efficiency of 10.4% at 20 mA continuous current with output power up to 9.3 mW for encapsulated AlGaN LEDs emitting at 278 nm (Shatalov et al. 2012). UV Craftory has developed commercial production of 50 mW AlGaN LEDs with wavelength ranging from 255 nm to 355 nm which have 10% external quantum efficiency (EQE) and over 10000 hours life time (Ippommatsu et al. 2013). For AlGaN lasers, the group of Technische Universität Berlin has reported laser grown on AlN bulk emitting at 279 nm with threshold of 50 mJ/cm^2 (IQE 20~30%), and laser grown on ELO (epitaxially laterally overgrown) AlN/sapphire template emitting at 272 nm with threshold of 65 mJ/cm^2 (IQE 10~20%). Both of two are TE-polarization dominant (Martens et al. 2014). (Xie et al. 2013) reported low threshold power of 84 kW/cm^2 for lasing at 280.8 nm and (Johnson et al. 2012) demonstrated lasing at 266 nm with threshold of 41 kW/cm^2. Both of devices are based on the AlGaN MQWs grown on single crystal AlN bulk substrates. To achieve IQE higher than 60%, AlN bulk single crystal can be used since its threading dislocation density is below 5×10^8 cm^{-2} (Hirayama et al. 2014), but it suffers from high impurity absorption, high cost and limited availability. Riken group has used ammonia pulsed-flow multilayer growth to fabricate AlN template on sapphire to obtain IQE of 60% from AlGaN QWs (Hirayama et al. 2007; Hirayama et al. 2014). Recently, for the devices grown on AlN templates on sapphire, simulated emission was observed at wavelengths of 256 nm and 249 nm with thresholds of 61 kW/cm^2 and 95 kW/cm^2 at room temperature, as reported by (X.-H. Li et al. 2014).

The development of III-nitride-based VCSELs includes optically-pumped devices at blue wavelengths (Redwing et al. 1996; Krestnikov & Ledentsov 1999), and room temperature CW lasing

VCSELs by current injection for blue/violet wavelengths (Higuchi et al. 2008; Lin et al. 2014; Kasahara et al. 2011). So far, no efficient VCSELs operating below 300 nm were reported.

One of the biggest challenges for UV VCSELs lies in the need for high reflectivity DBRs. Conventional AlInGaN based DBRs have been explored to give high reflectivity from blue to the near-UV region. For example, 25-pair $Al_{0.18}Ga_{0.82}N/Al_{0.8}Ga_{0.2}N$ has a reflectivity as high as 99% with bandwidth of 26 nm at central wavelength of 347 nm (Mitrofanov et al. 2006). Below 300 nm, (Moe et al. 2006) have demonstrated reflectivity of 66% and 83% for the shortest wavelengths of 245 nm and 279 nm, using 10 and 21 pairs of AlGaN/AlN, respectively. It is difficult to achieve high reflectivity requirement due to large absorption and small refractive index contrast of the materials in DUV region. Conventionally used AlGaN layers exhibit large lattice mismatch as high as ~2.4% between GaN and AlN to achieve only small refractive index contrast in the mirror structure. The high reflectivity requiring large number of pairs was accompanied by the dislocations, cracks or rough interfaces. So the novel system is necessary to build efficient DBR structures below 300 nm.

In this thesis, BAlGaN material system would be used to achieve the target. The primary reason for the B incorporation is that a very small amount of B in AlN could introduce a strong refractive index contrast (Watanabe et al. 2003; Abid et al. 2012). For example, BAlN with only 1.2% B can have a refractive index contrast of 0.17 with AlN. Besides, BAlN system exhibits less optical absorption than AlGaN due to its large bandgap. Additionally, both the large refractive index contrast and strain-compensated structure could be obtained at the same time by alternating BAlN and AlGaN layers in the DBR.

4 METHODOLOGY

The growth was performed in a MOVPE T-shape reactor (Gautier et al. 2007) under 100 Torr. Hydrogen was used as carrier gas. Trimethyl-aluminum (TMAl), thrimethyl-gallium (TMGa), triethylborane (TEB) and NH_3 were used as precursors for aluminum, gallium, boron and nitrogen, respectively. 900-nm thick AlN templates on c-axis sapphire and 3 μm GaN templates on c-axis sapphire were used as substrates.

High resolution X-ray diffraction (XRD) measurements were performed in a Panalytical X'pert Pro MRD system with Cu Kα radiation to determine composition and other structural information. The depth concentration profiles for different elements were performed by secondary ion mass spectroscopy (SIMS) analysis.

Surface morphology was characterized by atomic force microscope (AFM) and scanning electron microscope (SEM). The sample was then prepared for scanning transmission microscopy (STEM) using focused ion beam (FIB) thinning and ionmilling. 100 nm carbon was deposited before FIB in order to protect the surface. High-angle annular dark field scanning transmission microscopy (HAADF-STEM) characterizations were performed on aberration-corrected JEOL 2200FS electron transmission microscope.

The optical properties were investigated by photoluminescence (PL) and depth-resolved cathodoluminescence (CL) techniques. The PL excitation at 266 nm was provided by the second harmonic generation of a continuous laser. The emission is analyzed by a 1 m focal length monochronometer and detected by a CCD camera. Both the optical excitation and light collection are from sample surface. Optical transmission measurements were performed under Xenon arc lamp excitation for determination of the absorption band-edge and absorption coefficients in the wells.

5 EXPECTED OUTCOME

This work is in the framework of developing DUV VCSELs based on new BAlGaN material system. The main research work includes AlGaN active region, bottom DBR based on new BAlGaN material and final laser devices. The expected outcome of this thesis contains following part:

- MOVPE growth study for AlGaN layers including a careful control of composition and strain state.
- Design and growth of AlGaN MQWs structure which preserves the oscillator strength of TE-polarized transition.
- MOVPE growth study for new BAlN material including its growth conditions and structural characteristics.
- Achievement of DUV DBRs based on BAlN/Al(Ga)N system.
- Realization of AlGaN-based DUV lasers, and BAlGaN-based RCLEDs and VCSELs.

6 STAGE OF THE RESEARCH

The whole work can be divided into three sections: AlGaN active region, BAlGaN DBRs and final devices. Obtained results are presented in subsection 6.1 and 6.2, while the next plans are listed in subsection 6.3.

6.1 DUV AlGaN MQWs

The first part was concentrated in the optimization of AlGaN layers and AlGaN MQWs emitting at 280 nm.

6.1.1 AlGaN Composition and Relaxation

In order to obtain a good control over composition and relaxation for AlGaN growth, a series of AlGaN single layers were grown on AlN templates. The relationship between composition and TMAl/III ratio as wells as thickness and relaxation has been established. For the fully-strained thin layers below critical thickness, Al composition in the solid phase varies linearly with the TMAl relative concentration shown in Fig. 1. Additionally, the AlGaN growth rate, shown in the inset, varies linearly with the total III elements flow (TMAl+TMGa) while the V/III ratio remains constant, which indicates that the growth occurs in a mass transport limited regime.

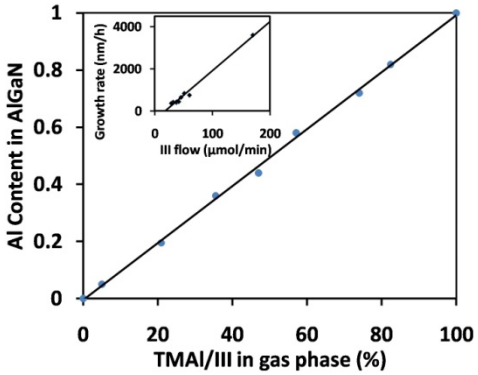

Figure 1: Al composition of AlGaN layers fully-strained on AlN templates Vs. TMAl/(TMAl+TMGa) ratio. The inset shows the growth rate versus total flow rate of (TMAl+TMGa).

However, when the thickness of the single AlGaN layer was increased under the same TMAl/III ratio so that the layer relaxed, it was observed that the average Al content in the layer decreased. This composition fluctuation during AlGaN relaxation has generally been ascribed to the composition pulling effect. G.B. Stringfellow *et al.* explained that the excess lattice mismatch energy would perturb the solid composition towards the composition which minimizes mismatch (G.B.Stringfellow 1993). The smaller adatoms will be incorporated preferentially at steps having relative compressive strain, and larger adatoms under relatively tensile strain (Tersoff 1996; Venezuela et al. 1999).

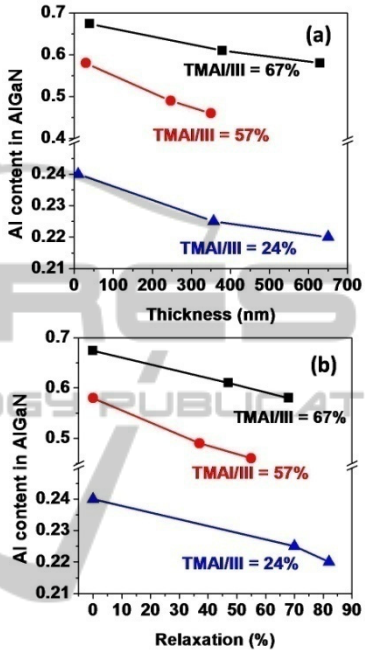

Figure 2: Al content in the AlGaN single layers plotted as a function of (a) layer thickness, and (b) corresponding layer relaxation for three different TMAl/(TMAl+TMGa) ratios.

Very few studies have considered AlGaN layers grown on AlN template which would be under compressive strain. In the present investigation, as shown in Fig. 2, a decrease in the Al composition of AlGaN layers is evidenced when the layer thickness (and hence the layer relaxation) is increased. For three different TMAl/III ratios in the gas phase, a clear Al content drop can be observed, confirming the composition pulling effect. In our case, AlGaN is under compressive strain on AlN, so in the initial stage when the layer is fully strained, AlGaN has a tendency towards higher Al content in order to minimize mismatch, while for the relaxed layer case, we see a lower Al content. Since Ga-N has a smaller bond energy than Al-N, Ga incorporation would be more controlled by the strain state than Al incorporation (Reuters et al. 2012; Bogusławski et al. 2000), which means that Ga atoms are expelled out for the initial stage under high compressive strain,

and Ga incorporation increases when the layer is relaxed with lateral lattice increasing.

6.1.2 TE-enhanced AlGaN MQWs Design

C-plane AlGaN alloys exhibit anisotropic optical polarization properties: E-field ⊥ c polarized emission (TE polarization) decreases when compared to the emission polarized along the c axis (E-field // c) as the Al composition increases for the deep UV wavelength, which is detrimental to surface-emission. This is attributed to the arrangement of the valence bands at the Γ point of Brillouin zone and Γ_7 symmetry becomes the upper valence band for an aluminum composition typically higher than 10% (Ryu et al. 2013; Kolbe et al. 2010; Nam et al. 2004; Leroux et al. 2004; Leroux et al. 2002). However, it is possible to restore the amplitude of the oscillator strength by imposing some strain in the AlGaN QW, which can affect the valence band states and the selection rules (Chuang & Chang 1996; Northrup et al. 2012; Ivanov et al. 2014; Murotani et al. 2011). The strain is due to the lattice mismatch between barriers and wells which have different Al content. Thus, the barrier composition can be chosen to provide sufficient compressive strain in the wells in order to enhance the TE-polarized optical transition.

To achieve emission at a wavelength of around 280 nm, the Al composition of the well was chosen to be x_{Al} = 0.37 and the well thickness was fixed to 1.7 nm in the calculations. The thickness of barriers was fixed to 10 nm. Envelop function simulations taking into account strain and built-in electric fields have been performed for AlGaN/AlGaN MQWs structure. The optimal Al content in barriers is designed to be 0.57 (±0.01), for which the strain (-0.5%) introduced in the wells is sufficient to preserve the oscillator strength of TE-polarized optical transition and therefore surface emission.

6.1.3 Growth and Characterizations of MQWs

In order to release the strain in the barriers, a relaxed $Al_{0.58}Ga_{0.42}N$ buffer was grown on AlN template as a pseudo-substrate. Then, 4-period $Al_{0.57}Ga_{0.43}N$ / $Al_{0.38}Ga_{0.62}N$ MQWs were grown on top based on the design. HAADF-STEM cross-section images of MQWs and upper part of the relaxed buffer were shown in Fig. 3(a) and 3(b). The barriers thickness is measured to be 10 ~ 11 nm from intensity profiles and the wells thickness is of 1.6 ~ 1.8 nm. The average composition of barriers could be determined from EDX quantitative analysis and was found to be 0.57 (± 0.015). Since the spatial resolution of the EDX analysis is typically of 2 nm, in order to determine the composition of ultra-thin wells, high-resolution Z-contrast HAADF-STEM image was transformed into quantitative composition mapping by following a procedure proposed in (Pantzas et al. 2012). The background intensity has been subtracted and thickness variation has been corrected. The complete analysis results in a chemical mapping were shown in Fig. 3(c). The average Al content in the barriers is accord with EDX value (x_{Al} ~0.57) and the average Al content in the wells is estimated to be x_{Al} ~0.38 (± 0.015). The thickness and composition values obtained from Figs. 3(a)-3(c) fit well the XRD experimental data.

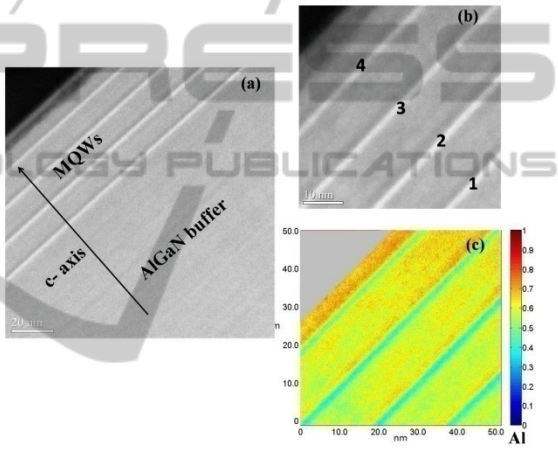

Figure 3: (a) Cross-section High-angle Annular Dark Field Scanning Transmission Electron Microscopy (HAADF-STEM) images taken along the <1 1 -2 0> zone axis for MQWs and buffer layer; (b) High magnification of HAADF-STEM images; (c) Al composition map obtained from (b).

Cathodoluminescence (CL) spectra at 77 K under different excitation energy have been shown in Fig. 4(a). Under a low excitation power of 3 keV corresponding to a penetration depth of the electron beam of typically 30 nm, a single emission peak from wells at 286 nm indicates that the carriers are mostly confined in the wells. When the excitation power is increased to 10 keV and the penetration depth of the excitation beam reaches 230 nm, a luminescence signal at 262 nm appears in addition to the emission of the wells, which is attributed to the barriers and buffer layer. The emission at 262 nm indeed corresponds to a bandgap energy of 4.73 eV, which is in agreement with the experimental composition of the barriers and buffer layer (x_{Al} ~ 0.57). At room temperature the increase of the

barrier luminescence with respect to 77K is attributed to the thermal activation of carriers in the AlGaN layers (barriers or buffer layers). In the case of an optical in-well pumping (excitation at 266 nm) as displayed in Fig. 4(b), the laser beam is mainly absorbed in the QWs and not in the barriers. Thus, only the luminescence of the wells is observed. However, it is found that both classical photoluminescence and cathodoluminescence provide the same QW emission line. The linewidth is 9.5 nm for PL at 77 K and 11.9 nm for PL at 300 K.

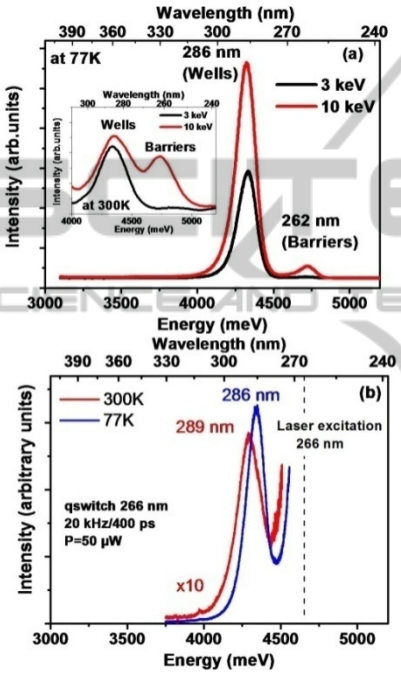

Figure 4: (a) Cathodoluminescence (CL) spectra at 77 K (and at 300 K in the inset) for two different values of excitation power; (b) Photoluminescence (PL) at 77 K and 300 K under excitation of 266 nm.

Figure 5 shows the macro-transmission measurements (E-field ⊥ c configuration) at 77 K together with numerical simulations based on transfer matrix formalism. The experimental spectrum reveals the absorption edge of the barriers at 260 nm, while a 10% drop of transmission is observed at 281 nm due to absorption in the wells. It is worth noting that calculations fit the experimental results in a satisfying way. The absorption coefficients used in the simulation are also displayed in Fig. 5 for both barriers and wells. A weak absorption with linear energy dependence has been added in the barriers and the buffer in order to reproduce the overall decrease of the transmission signal. The latter might be caused by defects originated from the AlN template. The absorption coefficient in the wells is found to be as high as 3×10^5 cm^{-1}, which implies that the oscillator strength is preserved in the QWs despite the high aluminium composition.

It is noted that the splitting between Γ_{7CH}-CB (fundamental) and Γ_9-CB transitions is evaluated to be equal to 32 meV. By considering the AlGaN broadening which is due to intrinsic alloy disorder and extrinsic inhomogeneities such as QW thickness fluctuations, it appears that the Γ_{7CH}-CB and Γ_9-CB transitions lie in the same energy range. The energy difference between these two transitions depends on several parameters (band offset, deformation potentials, effective masses…). So the absorption signal accounts for both transitions. However, it has been established through calculations that the strain preserves the oscillator strength of the fundamental transition (Γ_{7CH}-CB). Therefore it can be concluded that our MQW design with the use of relaxed buffer is promising for the fabrication of surface-emitting LED or lasers in DUV region.

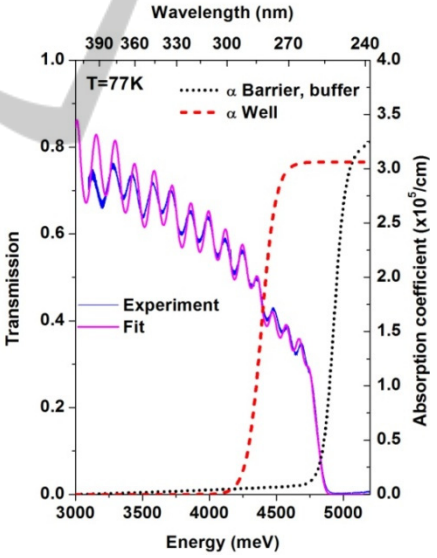

Figure 5: Macro-transmission measurements and transfer-matrix simulation of MQWs together with absorption coefficients (α_{well}, $\alpha_{barrier, buffer}$) used in the simulation.

More details can be found in (X. Li, Sundaram, Disseix, et al. 2015).

6.2 MOVPE Growth Study of BAlN

The second part of this work focuses on the study of BAlN layers grown by MOVPE.

6.2.1 BAlN Thin Layers

Wurtzite BAlN layers with boron composition as high as 12% were successfully grown by MOVPE. The growth was performed at 650˚C and then annealed at 1020˚C. Under high TEB/III ratio of 39%, as shown in Fig. 6(a), BAlN single layer grown on GaN templates at 650˚C with 20 nm thickness demonstrates an X-ray diffraction peak at 36.38˚ (± 0.17˚), which indicates that the layer has smaller lattice c than AlN due to boron substituting Al atoms in the crystal structure. We can assume the layer is fully-relaxed considering the large lattice mismatch between BAlN layer and GaN template. In this case, the c-lattice constant is 4.935 Å (± 0.022 Å), which corresponds to boron composition of 5.6% (± 2.8%) by applying Vegard's Law. The complete relaxation of the layer can be confirmed in Fig. 7: when we stop TEB flow and only grow AlN layer, the 2θ-ω peak of the layer is located at 36.02˚ corresponding to completed relaxed AlN layer.

When the deposition temperature is increased, shown in Fig. 6(b), the BAlN peak is weakened, and then disappears when it is increased to 800˚C. It indicates that under this high TEB/III ratio the crystallinity is worse when the layer is grown at higher temperature. Low temperature growth can alleviate B-rich phase poisoning issue under high TEB/III ratio.

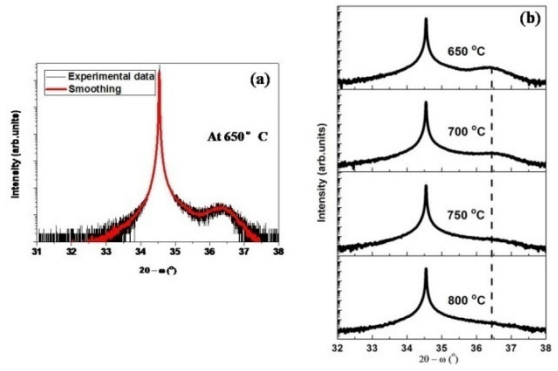

Figure 6**:** (a) HR-XRD 2θ-ω scan of 20 nm BAlN layers grown on GaN template at 650 °C under TEB/III=39%; (b) shows the influence of growth temperature which was varied between 650°C to 800°C.

In order to have different amount of boron incorporation, a series of samples were grown on GaN templates by continuous method, and TEB/III ratio was changed run to run. As shown in Fig. 7, when TEB/III ratio is increased from 0 to 39%, the peak of the layer shifts gradually towards greater diffraction angles (0 to 5.6% boron). The peak is

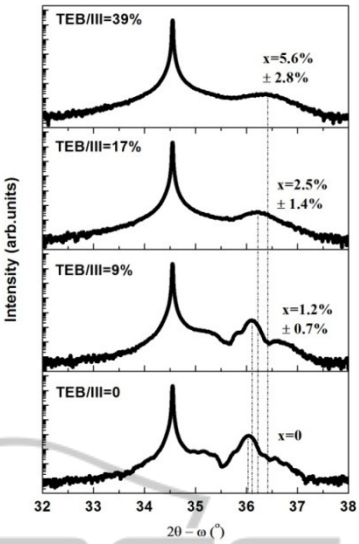

Figure 7: HR-XRD 2θ-ω scans of 20 nm BAlN grown on GaN templates by continuous method under different TEB/III ratio.

broadened with fringes missing due to polycrystalline nature of BAlN.

BAlN single layers with clear defined X-ray diffraction peaks were also achieved by flow-modulate method on AlN templates which are appropriate substrates for deep UV devices, as well as on GaN templates in order to distiguish the XRD peak of BAlN from the substrate peak. As shown in Fig. 8, clear XRD peaks can be identified at 36.59˚ (± 0.20˚) on both GaN and AlN templates. Lattice c is 4.908 Å (± 0.025 Å) and the corresponding boron content is 9% (± 3.2%). Since BAlN peak is very close to AlN template peak, the deconvolution of substrate peak and layer peak is shown in the inset figure.

The concentration calculated by XRD has a large error range because of the broadness of the BAlN diffraction peak and uncertainty of the lattice parameters and strain. These all influence calculation of the composition from diffraction peak positions, especially for the layer with high boron content. So the boron incorporation into the layer was also analysed by SIMS profile along the growth direction in Fig. 9. The Al signal is decreased in the BAlN layer compared with the signal of the template indicating that boron atoms were substitutionally incorporated into AlN lattice. Boron has a uniform distribution along the growth direction. The concentration of boron can be calculated based on atomic concentration obtained by SIMS. In order to calibrate the SIMS signal for quantitative measurements, a boron-implanted AlN sample with

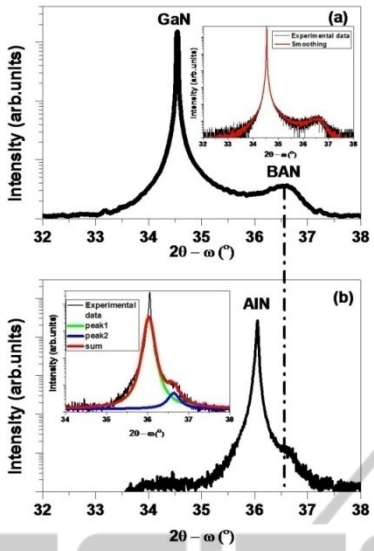

Figure 8: HR-XRD of 70 nm BAlN on (a) GaN template and (b) AlN template by FME growth (TEB/III=39%). Inset figures show the smoothing and deconvolution of two peaks.

known boron content was used as a reference. The concentration of boron calculated from the SIMS signal is 12% with 0.6% error (inset of Fig. 9), which agrees with the composition range given by XRD diffraction peak positions (6% ~12%).

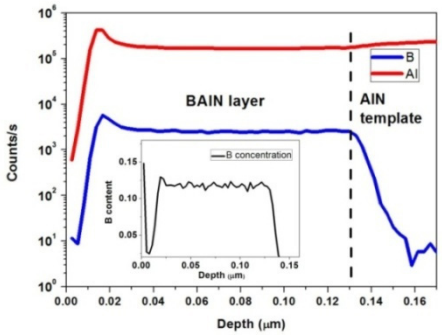

Figure 9: SIMS elemental concentration depth profiles of B and Al for the sample grown on AlN template; inset shows the boron concentration obtained by using boron implanted AlN as calibration sample.

More details can be found in (X. Li, Sundaram, El Gmili, et al. 2014). The promising results advance prospects for MOVPE-grown boron alloys, which can result in more freedom in bandgap, strain engineering with tailoring of refractive index of DBR structures for eventual deep-UV sources.

6.2.2 BAlN Heterostructure

Low temperature growth can alleviate the boron poisoning issue, but it does not facilitate AlN growth for the heterostructure. The fabrication of the heterostructure is an important issue which needs to be further developed no matter for BAlGaN-based MQWs or for DBRs. In this subsection, 5-period AlN/BAlN heterostructure was grown at 1000˚C. Flow-modulate method was applied during BAlN growth.

The boron concentration in the BAlN layers along growth direction was evaluated by SIMS profile, as shown in Fig. 10(a). It was clear that B profile varies anti-phase with Al, which indicates that Boron atoms substitute Al atoms on the III sites of lattice to form alloy. 5-period AlN/BAlN layers exhibit good uniformity except that the first AlN layer has lower AlN intensity which is due to some Ga contamination from the sample holder and the reactor (Kim et al. 2014). The boron content distribution along the growth direction was presented in Fig. 10(b). Under our growth conditions, 11% (± 0.6%) boron incorporation has been obtained.

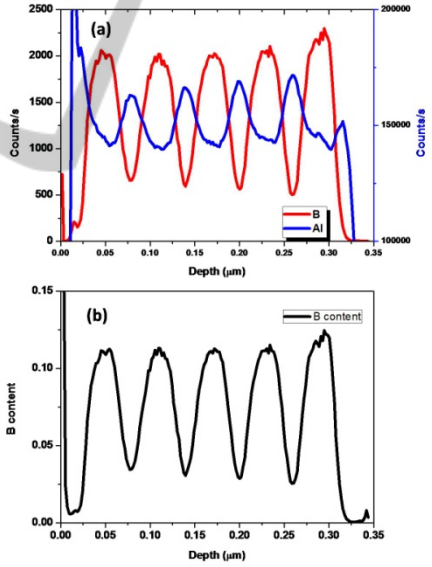

Figure 10: (a) SIMS elemental concentration depth profiles of B and Al for the sample grown on GaN template; (b) Boron content in solid layers calculated from SIMS by using boron implanted AlN sample as reference.

In order to investigate structural quality of this heterostructure and also crystalline characteristics, the cross-section STEM was performed along <1 1 -2 0> zone axis. As shown in Fig. 11(a), the bright-field STEM image shows that the AlN/BAlN heterostructure has columnar polycrystalline features, such as the part in the rectangle box. By looking into

the higher magnification image of the interface between 1st AlN and 1st BAlN in Fig. 11(c), it is clear that the 1st AlN layer is still monocrystalline. When BAlN growth starts, the lattice is oriented along c-axis for around 5 nm, and then the tilt as large as 60˚ can be observed which means the structure tends to be polycrystalline and columnar growth starts. Better contrast of AlN and BAlN layers can be observed by Z-contrast HAADF-STEM image shown in Fig. 11(b), where layers with higher brightness represent AlN layers and darker layers represent BAlN.

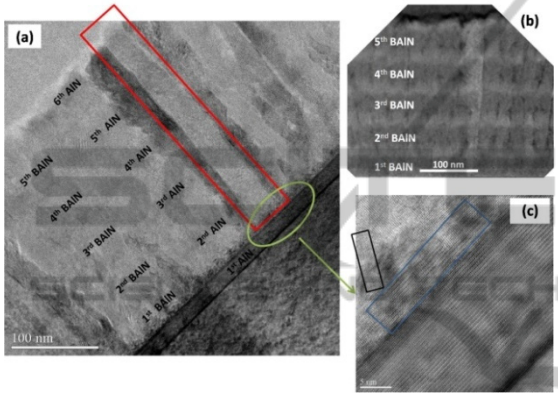

Figure 11: (a) STEM images (bright field) of 5-period AlN/BAlN heterostructure and columns are clearly observed in the structure; (b) HAADF-STEM image to show better contrast of BAlN and AlN layers; (c) high magnification of the zone where the 1st BAlN layer start to grow.

The polycrystalline feature was caused by the short diffusion length of boron atoms, which would challenge the applications of this material. From STEM image, we observed that the monocrystalline critical thickness for BAlN with 11% boron is around 5 nm, above which the polycrystalline growth occurs. Meanwhile, the monocrystalline critical thickness is around 500 nm for BAlN containing 2% boron as reported in the literature (Akasaka & Makimoto 2006). The more boron is incorporated, the smaller monocrystalline thickness of BAlN is. Therefore, for different applications, a compromise can be achieved between thickness and boron composition. For example, for deep UV DBRs, boron incorporation no more than 5% is enough to achieve high refractive index contrast (Watanabe et al. 2003; Abid et al. 2012). So the boron content can be decreased to maintain BAlN layers (30~40nm) monocrystalline. For ultra-thin layers such as MQWs or strain engineering superlattices, high boron incorporation can be used allowing a large design freedom and it can still be kept as monocrystalline for its thin thickness (below 10 nm).

More details can be found in (X. Li, Sundaram, El Gmili, et al. 2014).

6.3 Next Plans

Based on the preliminary results obtained, the next steps would involve:

1. Design and realization of BAlN/AlGaN DBRs with reflection at 280 nm. DBRs with high boron content and polycrystalline feature will be grown firstly. Then low boron would be used in order to reduce the interface and surface roughness. Meanwhile, AlGaN/AlN DBRs would also be optimized as a reference.
2. Fabrication and tests of final laser devices including laser diodes, RC-LEDs and VCSELs.

ACKNOWLEDGMENT

This work is supported by French ANR (Agence Nationale de la Recherche) in the framework of VESUVE project (ANR-11-BS03-0012). The authors would like to thank David Troadec from IEMN in Lille for FIB preparation.

REFERENCES

Abid, M. et al., 2012. *Distributed Bragg reflectors based on diluted boron-based BAlN alloys for deep ultraviolet optoelectronic applications*. Applied Physics Letters, 100(5), p.051101.

Akasaka, T. & Makimoto, T., 2006. *Flow-rate modulation epitaxy of wurtzite AlBN*. Applied Physics Letters, 88(4), p.041902.

Akasaki, I. et al., 1995. *Stimulated emission by current injection from an AlGaN / GaN / GaInN quantum well device*. Japanese Journal of Applied Physics, 34, p.1517.

Bogusławski, P., Rapcewicz, K. & Bernholc, J.J., 2000. *Surface segregation and interface stability of AlN/GaN , GaN/InN , and AlN/InN {0001} epitaxial systems*. Physical Review B, 61(16), pp.820–826.

Chuang, S.L. & Chang, C.S., 1996. *K□P Method for strained wurtzite semiconductors*. Physical Review B, 54(4), pp.2491–2504.

Ding, J. et al., 1990. *Laser action in the blue-green from optically pumped (Zn,Cd)Se/ZnSe single quantum well structures*. Applied Physics Letters, 57(26), pp.2756–2758.

G.B.Stringfellow, 1993. *Compositional ordering in semiconductor alloys*. Mater. Res. Soc. Symp. Proc., 312, pp.35–46.

Gautier, S. et al., 2007. *GaN materials growth by MOVPE in a new-design reactor using DMHy and NH3*. Journal of Crystal Growth, 298, pp.428–432.

Gil, B., 1998. *Group III nitride semiconductor compounds*, Clarendon Press.

Han, J. et al., 1998. *AlGaN/GaN quantum well ultraviolet light emitting diodes*. Applied Physics Letters, 73(12), p.1688.

Higuchi, Y. et al., 2008. *Room-temperature CW lasing of a GaN-based vertical-cavity surface-emitting laser by current injection*. Applied Physics Express, 1, p.121102 1–3.

Hirayama, H. et al., 2007. *231–261 nm AlGaN deep-ultraviolet light-emitting diodes fabricated on AlN multilayer buffers grown by ammonia pulse-flow method on sapphire*. Applied Physics Letters, 91(7), p.71901.

Hirayama, H. et al., 2014. *Recent progress and future prospects of AlGaN-based high-efficiency deep-ultraviolet light-emitting diodes*. Japanese Journal of Applied Physics, 53(10), p.100209.

Ippommatsu, M. et al., 2013. *Development of AlGaN DUV-LED*. In *10th Conference on Lasers and Electro-Optics Pacific Rim (CLEO-PR)*.

Ivanov, S.V. et al., 2014. *Plasma-assisted molecular beam epitaxy of Al(Ga)N layers and quantum well structures for optically pumped mid-UV lasers on c-Al_2O_3*. Semiconductor Science and Technology, 29(8), p.084008.

Johnson, N.M. et al., 2012. In *paper presented at the 9th International Symposium on Semiconductor Light Emitting Devices, Berlin*.

Kasahara, D. et al., 2011. *Demonstration of blue and green GaN-based vertical-cavity surface-emitting lasers by current injection at room temperature*. Applied Physics Express, 4(7), p.072103 1–3.

Kim, J. et al., 2014. *Origins of unintentional incorporation of gallium in InAlN layers during epitaxial growth, part II: Effects of underlying layers and growth chamber conditions*. Journal of Crystal Growth, 388, p.143-149.

Kolbe, T. et al., 2010. *Optical polarization characteristics of ultraviolet (In)(Al)GaN multiple quantum well light emitting diodes*. Applied Physics Letters, 97(17), p.171105.

Krestnikov, I.L. & Ledentsov, N.N., 1999. *Photopumped InGaN / GaN / AlGaN Vertical Cavity Surface Emitting Laser Operating at Room Temperature*. phys. stat. sol., 511, pp.511–516.

Leroux, M. et al., 2004. *About some optical properties of $Al_xGa_{1-x}N$ /GaN quantum wells grown by molecular beam epitaxy*. Superlattices and Microstructures, 36, pp.659–674.

Leroux, M. et al., 2002. *Optical characterization of $Al_xGa_{1-x}N$ alloys ($x<0.7$) grown on sapphire or silicon*. Physica Status Solidi (b), 234(3), pp.887–891.

Li, X., Sundaram, S., Disseix, P., et al., 2015. *AlGaN-based MQWs grown on a thick relaxed AlGaN buffer on AlN templates emitting at 285 nm*. Optical Materials Express, 5(2), pp.380-392.

Li, X., Sundaram, S., El Gmili, Y., et al., 2014. *BAlN thin layers for deep UV applications*. In *E-MRS Spring Meeting*.

Li, X., Sundaram, S., El Gmili, Y., et al., 2014. *MOVPE grown periodic AlN/BAlN heterostructure with high boron content*. Journal of Crystal Growth, pp.3–6.

Li, X.-H. et al., 2014. *Low-threshold stimulated emission at 249 nm and 256 nm from AlGaN-based multiple-quantum-well lasers grown on sapphire substrates*. Applied Physics Letters, 105(14), p.141106.

Lin, B.C. et al., 2014. *Design and fabrication of a InGaN vertical-cavity surface-emitting laser with a composition-graded electron-blocking layer*. Laser Physics Letters, 11(8), p.085002.

Martens, M. et al., 2014. *Performance characteristics of UV-C AlGaN-based lasers grown on sapphire and bulk AlN substrates*. IEEE Photonics Technology Letters, 26(4), pp.342–345.

McIntosh, F.G. et al., 1996. *Growth and characterization of AlInGaN quaternary alloys*. Applied Physics Letters, 68(1), p.40.

Mitrofanov, O. et al., 2006. *High-reflectivity ultraviolet AlGaN/AlGaN distributed Bragg reflectors*. Applied Physics Letters, 88(17), p.171101.

Moe, C.G. et al., 2006. *AlGaN/AlN distributed bragg reflectors for deep ultraviolet wavelengths*. Physica Status Solidi (a), 203(8), pp.1915–1919.

Murotani, H. et al., 2011. *Silicon concentration dependence of optical polarization in AlGaN epitaxial layers*. Applied Physics Letters, 98(2), p.021910.

Nam, K.B. et al., 2004. *Unique optical properties of AlGaN alloys and related ultraviolet emitters*. Applied Physics Letters, 84(25), pp.5264–5266.

Northrup, J.E. et al., 2012. *Effect of strain and barrier composition on the polarization of light emission from AlGaN/AlN quantum wells*. Applied Physics Letters, 100(2), p.021101.

Pantzas, K. et al., 2012. *Nanometer-scale, quantitative composition mappings of InGaN layers from a combination of scanning transmission electron microscopy and energy dispersive x-ray spectroscopy*. Nanotechnology, 23(45), p.455707.

Redwing, J.M. et al., 1996. *An optically pumped GaN–AlGaN vertical cavity surface emitting laser*. Applied Physics Letters, 69(1), pp.1–3.

Reuters, B. et al., 2012. *Relaxation and critical strain for maximum In incorporation in AlInGaN on GaN grown by metal organic vapour phase epitaxy*. Journal of Applied Physics, 112(9), p.093524.

Ryu, H.-Y. et al., 2013. *Investigation of light extraction efficiency in AlGaN deep-ultraviolet light-emitting diodes*. Applied Physics Express, 6, p.062101.

Shatalov, M. et al., 2012. *AlGaN deep-ultraviolet light-emitting diodes with external quantum efficiency above 10%*. Applied Physics Express, 5, p.082101.

Shatalov, M. et al., 2002. *Deep ultraviolet light-emitting diodes using quaternary AlInGaN multiple quantum wells*. IEEE Journal of Selected Topics in Quantum Electronics, 8(2), pp.302–309.

Tersoff, J., 1996. *Stress-driven alloy decomposition during step-flow growth*. Physical review letters, 77(10), pp.2017–2020.

Venezuela, P. et al., 1999. *Self-organized growth of alloy superlattices*. Letters to nature, 397, pp.678–681.

Watanabe, S. et al., 2003. *Refractive indices of $B_xAl_{1-x}N$ (x= 0-0.012) and $B_yGa_{1-y}N$ (y= 0-0.023) epitaxial layers in ultraviolet region*. Physica Status Solidi (c), 0(7), p.2691-2694.

Xie, J. et al., 2013. *Lasing and longitudinal cavity modes in photo-pumped deep ultraviolet AlGaN heterostructures*. Applied Physics Letters, 102(17), p.171102.